Advanced Powder Technology 34 (2023) 104263

Contents lists available at ScienceDirect

Advanced Powder Technology

journal homepage: www.elsevier.com/locate/apt

Original Research Paper

Making ultra-high strengthening and toughening efficiency in hybrid reinforcing of aluminum laminated composites via dispersion engineering

Behzad Sadeghi, Pasquale Cavaliere *

Department of Innovation Engineering, University of Salento, Via per Arnesano, 73100 Lecce, Italy

ARTICLE INFO

Article history:
Received 22 May 2023
Received in revised form 25 September 2023
Accepted 21 October 2023

Keywords:
Strength-ductility
metal-matrix composites
Al3BC nanoparticles
Interfacial strength
Dislocations distribution

ABSTRACT

To overcome the strength-ductility trade-off dilemma, herein we propose a hybrid in-situ/ex-situ reinforced aluminum matrix composite to achieve a uniform dispersion of reinforcements and strong reinforcement-matrix interfacial bonding. To exploit the pros of inter/intra granular dispersion of reinforcements, nano- Al_3BC particles have been in-situ synthesized into ultrafine-grained (UFG) Al grain interior reinforced by carbon nanotubes (CNTs) via an elemental powder mixture, mechanical activation and subsequent annealing process. The in-situ nano-scaled Al_3BC were uniformly distributed inside the elongated ultrafine Al grains, enabling stronger dislocation pinning and retention, providing stronger effective stress which consequently helps to enhance strength and strain hardening. The as-fabricated (Al_3BC, CNT)/UFG Al exhibits simultaneous enhancement in strength (394 MPa) and total elongation (19.7 %) compared with its counterpart without the nano-Al_3BC, suggesting the promising strengthening effects of in-situ/ex-situ reinforcing benefitting from the uniform dispersion and the strong semi-coherent interface with the matrix.

1. Introduction

Hybrid reinforcing is novel and significant strategy with the core idea of the hybrid reinforcements to exert their respective advantages, and to fabricate advanced metal matrix composites (MMCs) that is nowadays motivated by the purpose to overcome the strength-ductility trade-off [1–5]. Thanks to the higher efficiency of nano-sized reinforcements compared to counterpart micron-sized ones [6], a step forward has been taken in the direction of simultaneous improvement of strength and ductility. Although, the use of ex-situ reinforcement nanoreinforcement always brings the dilemma of uniform dispersion in MMCs [7,8]. Along with all the advantages of using ex-situ reinforcements, deleterious aspects such as the formation of incoherent interfaces between the reinforcement-matrix, the essence of problems such as stress concentration and deformation discontinuity at the microscale scale during the deformation process come out [9,10]. Therefore, it seems that the simultaneous use of the benefits of in-situ and ex-situ reinforcements as a hybrid reinforcing strategy would be one of the optimal ways to realize the simultaneous improvement of strength and ductility in MMCs. The essence of having a laminated structure accompanied with hybrid reinforcing significantly contributes to hetero-deformation induced (HDI) stress strengthening and sustained strain hardening, making the key mechanical properties of GNS-Cu/Al. What's more, high-performance reinforcing and a tailored architecture has been gianed in reduced graphene oxide (RGO)-CNT hybrid /Al composite prepared by a composite flake assembly process due to the formation of a planar network of RGO and CNT, which improves the load transfer efficiency between the matrix and the reinforcement in composites [5]. Recently, a strong but tough aluminum matrix composite (AMC) reinforcing with graphene oxide (GO)-CNT hybrid were prepared by powder metallurgy [4]. The strength of the composites was improved by the synergistic effect of carbon nanotubes, in-situ Al_3C_4 and GO. Very recently, superior tensile properties of AMC reinforced by both in-situ Al_2O_3 nanoparticles and ex-situ GNSs was developed via manipulating the PM route [11]. The composite possesses a high tensile strength of 464 MPa and appreciable amount of ductility (8.9 %), resulted from the combination effect of grain refinement, in-situ Al_2O_3 nanoparticles and exsitu GNSs. It is inferred the presence of a synergetic strategy between in-situ and ex-situ reinforcements accompanied with a tailored architecture could provide significant contribution of both

* Corresponding author.
E-mail address: pasquale.cavaliere@unisalento.it (P. Cavaliere).

https://doi.org/10.1016/j.apt.2023.104263

Nomenclature

α_i	The *i*'th parameter of the vdW interaction model, (–)
β	Stretching exponent, (–)
ϵ	Lennard-Jones potential characteristic energy, (J/mol)
γ	Angle between two vectors, (–)
Γ_{12}	Center-center distance between aggregates, (m)
ν	Frequency of electrostatic interaction, (–)
ρ_i	The *i*'th particle atom number density, (m^{-3})
σ	Lennard-Jones potential characteristic distance, (m)
θ	Angle between two vectors, (–)
ε_i	The *i*'th particle dielectric constant, (–)
φ	Aggregate's packing factor, (–)
$\vec{M}$	Rotation matrix, (–)
ξ	Aggregate's large scale cut-off chracteristic distance, (–)
A_{13}	Anisotropy coefficient, (–)
A_{Ham}	Hamaker's constant, (J)
C	London dispersion coefficient, ($J{\cdot}m^6$)
d	Center-center distance, (m)
D_f	Aggregate's fractal dimension, (–)
D_v	Volume-equivalent diameter, (m)
F	Interaction force, (N)
g	Radial distribution function, (–)
h	Planck's constant, ($m^2{\cdot}kg{\cdot}s^{-1}$)
I	Aggregate's inertia moment, ($kg{\cdot}m^2$)
k_B	Boltzmann's constant, ($m^2{\cdot}kg{\cdot}s^{-2}{\cdot}K^{-1}$)
k_f	Aggregate's fractal prefactor, (–)
m_i	The *i*'th particle's mass, (kg)
N_p	Number of primary particles, (–)
n_z	Number z-planes, (–)
$n_{s,xy}$	Number spheres in xy plane, (–)
r	Radial distance, (m)
r_s	Radius of a circle, (m)
$R_{\max}$	Aggregate's maximum radius, (m)
R_g	Aggregate's gyration radius, (m)
R_i	The *i*'th eigenvalue of the inertia moment matrix, (–)
R_{pi}	The *i*'th primary particle radius, (m)
T	Absolute temperature, (K)
V	Aggregate's volume, (m^3)
V_a	Aggregate's total volume, (m^3)
V_i	The *i*'th particle volume, (m^3)
V_p	Primary particle volume, (m^3)
W	Interaction energy, (J)

strengthening and toughening mechanisms to achieve the best combination of strength-ductility. Promisingly, the configuration of microstructure in mesoscale and uniform spatial distribution of hybrid reinforcements offer additional potential in tuning the mechanical properties of advanced AMCs [12]. Motivated by the above considerations, an easy and innovative route on basis of elemental powder strategy to in-situ-synthesize was employed to introduce nano-Al_3BC into AMCs reinforced with CNT to attain a significant synergy of high strength and toughness. In the present work, a smart and efficient way of powder metallurgy (PM) (referred to as flake PM in the literature [1,13–16]) was developed by combining high-speed predispersion and dual-speed ball milling (low speed ball milling (LSBM) & high speed ball milling (HSBM)) to produce (CNT, Al_3BC)/Al composites, in which the CNTs were first mechanically deagglomerated and uniformly coated onto the surface of the flake Al powder via the dry particle coating mechanism in a fast and uniform dispersion and better protection for the CNTs from subsequent damage. The formation of a composite between the reinforcing phase and the matrix involves a series of steps, including material selection, powder preparation, dispersion, mechanical milling, and subsequent annealing. In this innovative process, the Al3BC nanoparticles were synthesized in-situ after the final processing step, the annealing process. Each step is critical to obtain a well-dispersed, homogeneous composite material with tailored properties, as your study shows. Accordingly, the combination of plastic deformation, strain hardening, and fragmentation ultimately leads to the formation of the composite. The reinforcing elements, such as Al3BC and CNTs, are integrated into the Al matrix, resulting in a composite material with a microstructure that improves the specific properties.

2. Experimental

The fabrication of (1 wt% Al_3BC, CNT 0.45 wt%)/Al composites include the high-speed shearing process for breaking CNTs clusters and B agglomerations uniformly coating on the surface of the Al flakes (Fig. 1a) and the micro-micro rolling (MMR) process (Fig. 1b) [17,18] for producing the laminated composites. Details of the experimental are given in the following. The atomized spherical pure Al powders (6 μm), amorphous boron, and the pristine MWCNTs (1.5 wt%, diameter: 30–50 nm, length: 0.3–0.5 μm), synthesized by means of chemical vapor deposition (CVD), were used as raw materials. Generally, CVD-grown CNTs have a few defects and significant amorphous carbon coating on the tube surface [19], which promote the formation of an Al_3C_4 and Al_3BC. The spherical Al powders is firstly ball milled at 120 rpm for 15 h to obtain the Al flakes with thickness about 300 nm (as shown in Fig. 1(a)). To accommodate a uniformly coated CNTs and B particles on the Al flakes, CNTs, Al flakes and B particles were firstly mixed in molar ratio of Al/B/CNT = 3/1/1 in an agate mortar, then high-shear pre-dispersion processed (at 1500 rpm, 30 min). The prepared flaky-shaped powders and 2 wt% stearic acid with a ball-to-powder ratio 20:1 was then treated by LSBM (LSBM: 10 h, 120 rpm) to mechanically activated nanocomposite building blocks (CNT, B @ Al flakes), followed by HSBM (HSBM: 0.5 h, 300 rpm) to fabricate Al@ (CNT, B) composite powder. In order to avoid self-ignition, the ground powders were taken out of the jar after the temperature (T) dropped to around room T (26°C). After degassing at 400 °C, the composites powders were compacted, vacuum sintered (600°C, 2 h) and extruded (420 °C, ratio of 25:1). Then to further consolidate the composite, the plate was firstly cold rolled (reduction of 50 %) at room T and subsequent annealing (at 800°C, 3 h, flowing argon) to synthesize in-situ Al_3BC. The final main composite contained 1 wt% Al_3BC, 0. 45 wt% CNTs, 0. 1 wt% Al_3C_4, and 2.6 wt%. Al_2O_3. For comparison, the 1.5 wt% CNT/Al without B addition was also fabricated with the same procedure.

Microstructural analyses were carried out using high-resolution transmission electron microscopy (HR-TEM, Talos F200X G2), scanning transmission electron microscopy (STEM), and electron backscattered diffraction (EBSD, NordlysMax3, Oxford, SEM equipped with EDAX Velocity Super EBSD detector with a length step of 40 nm). Grain diameters were estimated by measuring the length and width at least 350 grains in EBSD images. The Raman spectroscopy using the 532 nm line of an Ar^+ laser as the excitation source and an electrochemical dissolution method [20] were used to evaluate the structural integrity of CNTs and the reaction between CNTs and Al. XRD analyses were performed using a

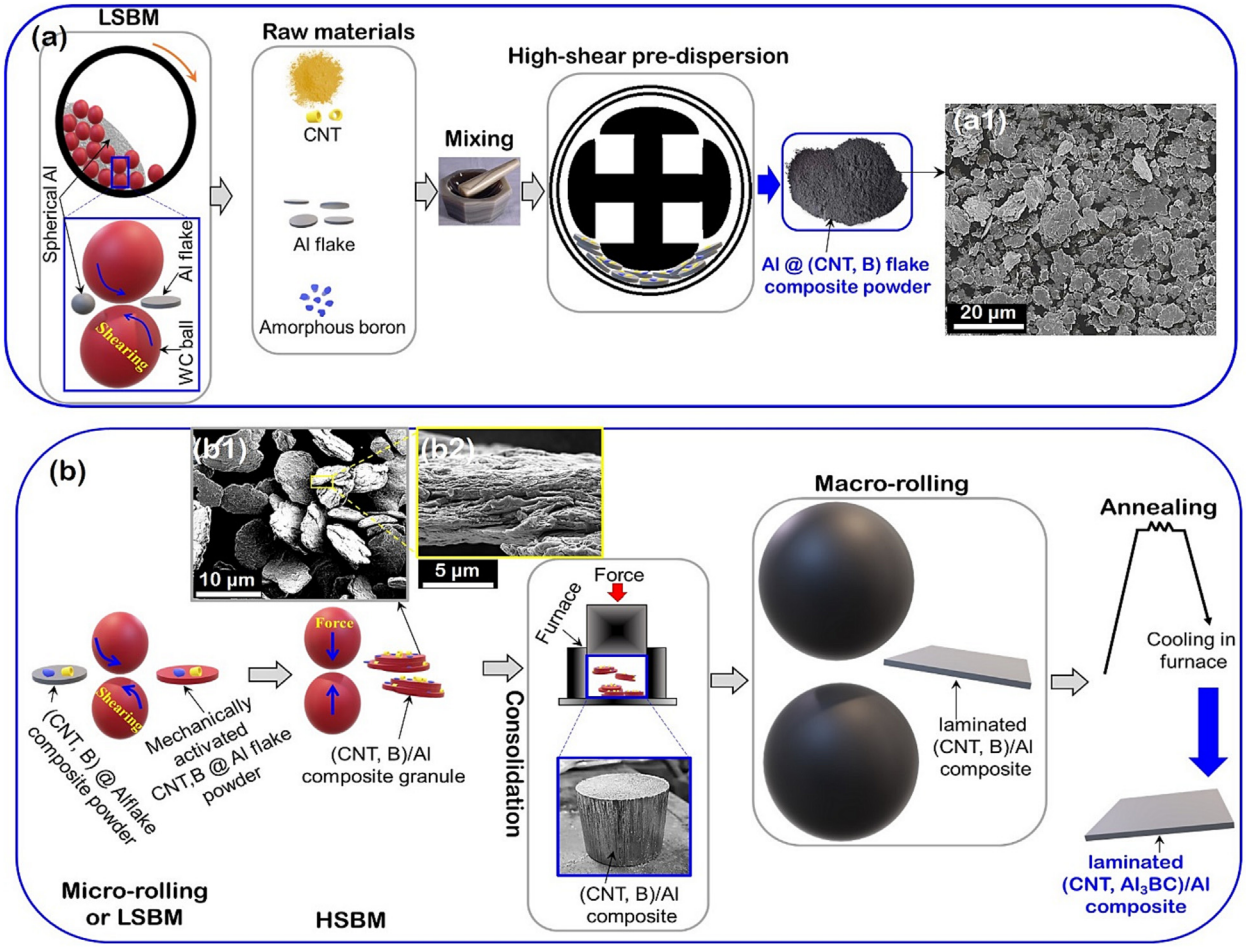

Fig. 1. Schematic diagram of (a) preparation of flaky-shape (CNT,B)@Al composite pawder (a1: SEM image of flaky-shaped Al particles), and (b) fabrication laminated (CNT, Al_3BC)/Al composites via micro–macro-rolling (MMR) process (b1,b2: SEM images of (b1) cold welded, and (b1)nanolaminated structure of each Al particles).

Rigaku D/Max-2500 X-ray diffractometer with Cu Kα (λ = 0.1540 6 nm) radiation. The dislocation density of samples was analyzed using [21]

$$\rho = \left(3\sqrt{2\pi}\langle\varepsilon^2\rangle^{1/2}\right)/(Db)$$

Where D is the equivalent average grain size, $\langle\varepsilon^2\rangle^{1/2}$ is the micro strain, ρ is the dislocation density, b is Burgers vector of Al, which is 0.286 nm [22]. The as-fabricated composite was sectioned into tensile specimens along the rolling direction (RD), and tensile tests were carried out at a constant strain rate of $1 \times 10^{-4}s^{-1}$ at room T.

3. Result and discussion

To obtain composite material fragments from raw powder through mechanical ball milling, several fundamental material science phenomena come into play. The powder deformation mechanism is dominated by the force, frequency of ball-to-powder collision and milling time [23,24]. Mechanical ball milling induces high-energy collisions between milling balls and powder particles, leading to plastic deformation (forming flaky shaped-powder particles especially in light alloys powders), work hardening, and fragmentation. Plastic deformation involves the permanent reshaping of materials without fracture, while work hardening increases material strength and hardness due to the accumulation of dislocations. In a planetary ball mill, there are two forces at play when things collide: one compressing force, and the other shearing force. The compressing force from balls impacting directly mostly makes the powder flattening, cold-welding, or even at larger rotational speed, and longer milling time, breaking into pieces. On the other hand, the shear force, which happens when balls impact from the side, rotate, or friction of balls, helps disperse nano particles evenly. All these processes are crucial for achieving a well-dispersed composite material with tailored properties. Moreover, subsequent annealing, if applied, further promotes bonding and consolidation. The present study the smart and efficient route adopted is used these scientific principles to create composite materials with improved characteristics.

Diffraction peaks of Al_3BC and Al were detected in (Al_3BC,CNT)/Al composite (Fig. 2b), while only Al peaks were found in (B,CNT)/Al composite (Fig. 2a). The formation of Al_3BC is mostly caused by the reaction Al particles with the B element and the carbon formed due to the decomposition of stearic acid during fabrication process, and subsequent annealing [25]. Indeed, due to the appearance of some area where boron and carbon atoms are supersaturated, Al_3BC particles are in-situ nucleated as homogeneously in solid state with a limited growth rate. In fact, due to very low solubility of boron and carbon atoms in Al especially at solid state reactions [26,27], the growth process of Al_3BC particles is soon compromised by the deficiency of carbon and boron atoms, consequently nanoscale Al_3BC particle are formed. However, the presence of Al_3C_4

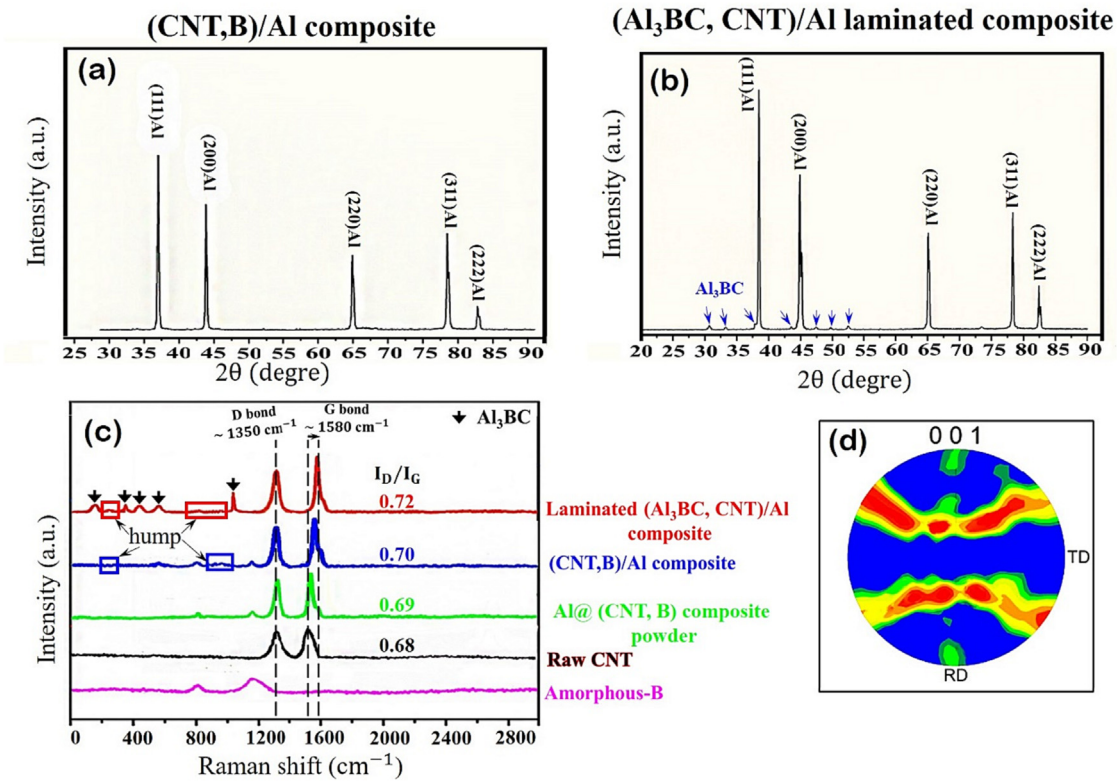

Fig. 2. (a,b)XRD spectra, and (c)Raman spectra of the understudy materials; (d) (001) pole figure of a typical (Al3BC,CNT)/Al laminated composite. (All the tested sample plane perpendicular to the RD).

effectively contribute to heterogeneously nucleate platelet Al_3BC particles with submicron size [28,29]. In this concept, It should be noted that the characteristic peaks of Al_3C_4 phase have not been observed in Al@(CNT,B) composite powder due to either very low relative content or the lack of formation. In addition, no specific peak of Al_3C_4 detected neither in the (CNT,B)/Al composite nor in the (Al_3BC,CNT)/Al laminated composite. This is more likely due to either no reaction between broken CNTs, or low relative content. Comparing the peaks intensity, one can be found that the ratio of {111} intensity to {200} increased after MMR process, developing a strong ⟨111⟩ fiber texture, verified by a typical (001) pole figure shown in Fig. 2d.

As shown in Fig. 2c, the relative intensity ratio of I_D/I_G of (Al_3BC, CNT)/Al composite increased to 0.72 while were 0.7, 0.69 and 0.68 for (CNT,B)/Al composite, Al@(CNT,B) composite powder and raw CNTs, which implies that there was almost no serious damage to CNTs during pre-dispersion, extrusion and MMR processes. In addition, only a peak shift of G-band from 1580 cm^{-1} to 1594 cm^{-1} was semi-quantitatively detected in the (Al_3BC, CNT)/Al composite, indicating might be originated from the infiltration of Al atoms in CNTs, causing slight distortion of sp^2 bonding structure of CNTs. The characteristic peaks of Al_3C_4 [30,31], were not detected in both (CNT,B)/Al composite and (Al_3BC,CNT)/Al composite. However, a few sluggish humps appeared in the composites indicates there may still exist slight interface reaction. It seems that thanks to the flaky-shaped Al building blocks and providing much more available effective surface, the deeper the CNTs are embedded into the Al particles, the smaller the growth value of I_D/I_G ratio, indication that the better the protection of the CNTs in both (CNT,B)/Al composite and (Al_3BC,CNT)/Al composite [8,32].

The images of SEM given in Fig. 3 a, b present the distribution of reinforcing phases in the matrix, in which the small-sized white phases distributing uniformly in the Al matrix are detected to be Al_3BC particles with the reference of the XRD and EDS results. High magnification image in Fig. 3c (brightfield STEM image) reveal that Al_3BC particles with almost spherical morphology are estimated their size are ranging from 20 to 30 nm.

Fig. 4a demonstrates an obvious laminated structure with the measured grain sizes are 190 and 545 nm. Such an observation is more likely to associate with the reduced grain boundary mobility and the subsequent restriction of grain growth rendered by the CNTs at the GBs. Furthermore, a more of the elongated grains possess a strong ⟨111⟩ texture with a few grains towards the ⟨001⟩ direction, indicating a strong restriction of slip both in and GBs of Al grains. The presence of a laminated microstructure with 40 % of low-angle GBs (LAGBs) which in turn composed of 12 % and 28 % with$\theta < 3°$ and $3° < \theta < 15°$, are strongly effective in manifesting a strong contribution of dislocations and LAGBs strengthening respectively (Fig. 4b). Furthermore, the presence of 60 % of HAGBs mostly decorated by CNTs and some γ-Al_2O_3 nanoparticles are more effective in blocking slipping dislocations, thereby forcing the dislocations to tangle and accumulate grain interior and near the boundaries with a very high density about 1.5×10^{16} m^{-2} (dashed ovals in Fig. 4 c).

A close look up the Fig. 4c, one can be found there are numerous spherical gray particles in size range of 6–25 nm, which are identified to be Al_3BC by STEM image given in Fig. 3d,j. thermodynamically, having a negative formation enthalpy — 56.34 KJ/mol [33] for Al_3BC compared to Al_3C_4 (— 36 KJ/mol [33]), availability of boron atoms with carbon atoms with uncompensated high energy electron bonds at damaged CNTs tips, and amorphous carbonas cover on CNTs, along with appropriate annealing heat treatment at 800°C for 3 h in flowing argon is ideal to in-situ synthesized Al_3BC nanoparticles. It is expected that the formation of the Al_3BC is

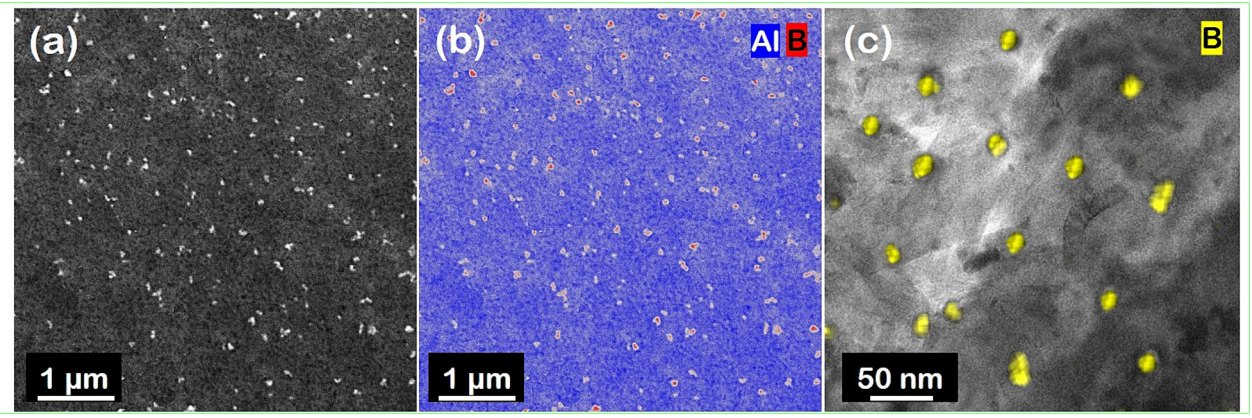

Fig. 3. The distribution of Al3BC in composite: (a) SEM image, (b) the corresponding binary image, and (c) EDS mapping incorporated into the brightfield image STEM.

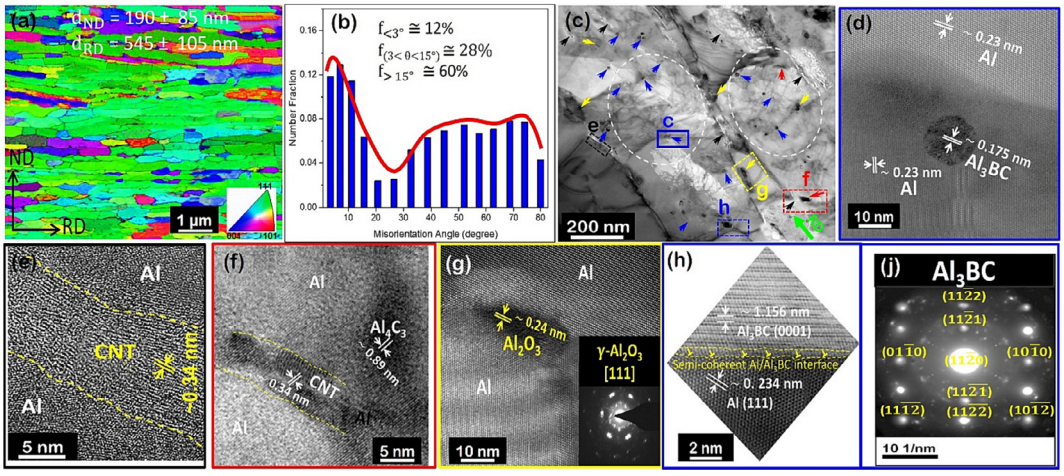

Fig. 4. (a)EBSD image of (Al_3BC,CNT)/Al laminated composite, (b) the distribution of the grain boundary misorientation angle (θ), (c)TEM image showing the elongated Al grains containing different reinforcing elements, (d)STEM image showing a nanoscale Al3BC in Al matrix, (e-h), HRTEM images of (e) CNT-Al interface, (f) a typical structure of CNT with small interfacial Al_4C_4, (g) structure of γ-Al_2O_3, (h) Al_3BC-Al interface formed in the grain interior of Al,(j) Relative Fast Fourier transforms of Al3BC. The dashed ovals showing dislocation entanglements. The red, black, blue and yellow arrows showing Al_4C_4, CNTs, Al3BC and γ-Al_2O_3, respectively. (For interpretation of the references to colour in this figure legend, the reader is referred to the web version of this article.)

mainly controlled by the diffusion rate of C and B in Al matrix, which should be increased with the T in solid states, so this is be more likely, no Al_3BC could form during hot extrusion. As soon as boron atoms run out, a few numbers of nanorod Al_4C_4 is formed due to exposure at high T. In other word, the Al_4C_4 content in this study not only depends on T as previously reported by [27], but also strongly depends availability of free boron and carbon atoms. The lattice fringes of an individual Al_3BC, CNT, Al_4C_4, and Al_2O_3 in the composites had a spacing of $\sim$ 0.175, 0.34 nm, 0.89 and 0.24 which approximately equals to that of the (110) plane of Al_3BC, (1120) plane of graphite, (003) plane of Al_4C_4, and (311) plane of γ-Al_2O_3, respectively (Fig. 4 d-g). Thus, it can be concluded that nanoscale Al_3BC with sizes of 6–25 nm respectively has been successfully synthesized in the composites. The relatively same size of Al_3BC nanoparticles previously in-situ synthesized by liquid–solid reaction [29], or by self-propagating high-T synthesis [34]. Contrary to complexity and expensive the other routes proposed, the synthesized route proposed in this paper is feasible and simple in which nanoscale Al_3BC is directly formed by the reaction between dissolved B and C atoms and Al matrix through ball milling and subsequent rolling and annealing. Due to the essence of having a strong interfacial bonding, good dispersion in the Al grain interior and complete single-crystal structure of in-situ Al_4C_3 nanoroads. Furthermore, the in-situ-Al_3BC/Al interface which has a semi-coherent bonding structure with orientation relationship (0111) Al_3BC // (1 1 1)Al, is contained with minimum number of mismatch dislocations at the interface (Fig. 3h) in line of the results in [35,36]. Such strong bonding strength accompanied with preferred orientation of both the elongated Al grains significantly guarantee the intragranular strengthening effects of Al_3BC on the elongated Al matrix. The CNTs mostly are embedded in Al matrix and aligned in the RD, signifying the existence of a strong and firm bounding between CNTs and Al matrix. The presence of a clean interface between CNT-Al with any void and interfacial product (Fig. 4 e) indicates not only a well-remaining of CNT structure with a strong bonding between Al and CNTs, but also strongly contributes in load transferring strengthening. However, small amount of nanoscale rod-like Al_4C_4 is in-situ formed by the reaction of partially damaged CNTs with Al matrix (red arrows in Fig. 4 f). Owing to interfacial Al_4C_4 preferentially nucleated at the open edges, so

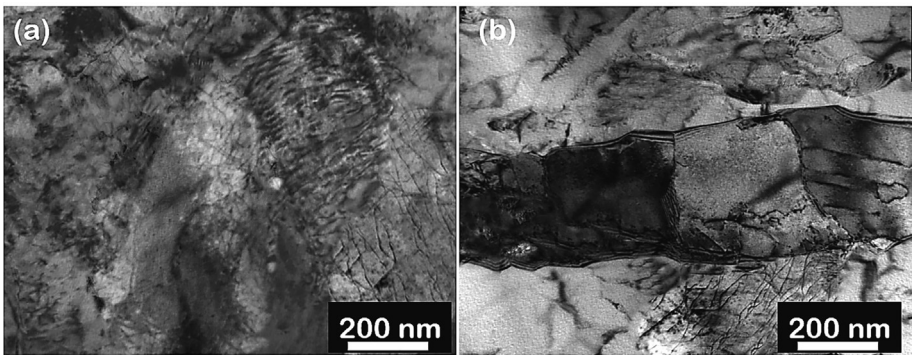

Fig. 5. TEM images of (a) (Al3BC,CNT/Al) and CNT/Al laminated composites, (b) CNT/Al composite; showing high density of dislocations.

Al_3C_4found at the open edges of CNTs which are more reactive than the CNT's parts in line of the results reported in [37,38]. It seems that the formation of Al_3C_4 could be related to shortening and breaking of CNTs, which in turn leading to an increasing number of carbon atoms available to react with Al and B in order to produce in-situ Al_3BC nanoparticles. Furthermore, some relatively spherical nanoparticles of γ-Al_2O_3 (Fig. 4 g) both in the Al grain interior and the GBs are existed (yellow arrows in Fig. 3c) as consequence of the transformation of native amorphous(am)-Al_2O_3 skin broken during processing at T > 450 °C[39]. Hence the oxygen introduced by the fabrication process almost effectively exists as oxides, e.g., γ-Al_2O_3. Consider the native Al_2O_3 skin on the surface of nanoflake is 4 nm thick, the volume of Al_2O_3 is about 2.6 vol% (8/300 × 100 % = 2.6 vol %) of the total volume of 300 nm nanoflake Al powder in agreement with the value of Al_2O_3 reported in [39]. By assuming all oxygen present is in am-Al_2O_3 completely transformed to γ-Al_2O_3 after annealing at 800°C, and also the oxygen content remains virtually unchanged after annealing. The nano-Al_3BC and Al_3C_4 play an important role for generating high effective stress via forest dislocation cutting and the Orowan strengthening, while the CNTs and nano-Al_2O_3 effectively provide a high back stress via accumulation and hindering of dislocation annihilation at the interfaces, and GBs. Precisely, a high dislocation density (8.13 × 10^{15} m^{-2}) mostly caused by inhomogeneous deformation between matrix

γγγ

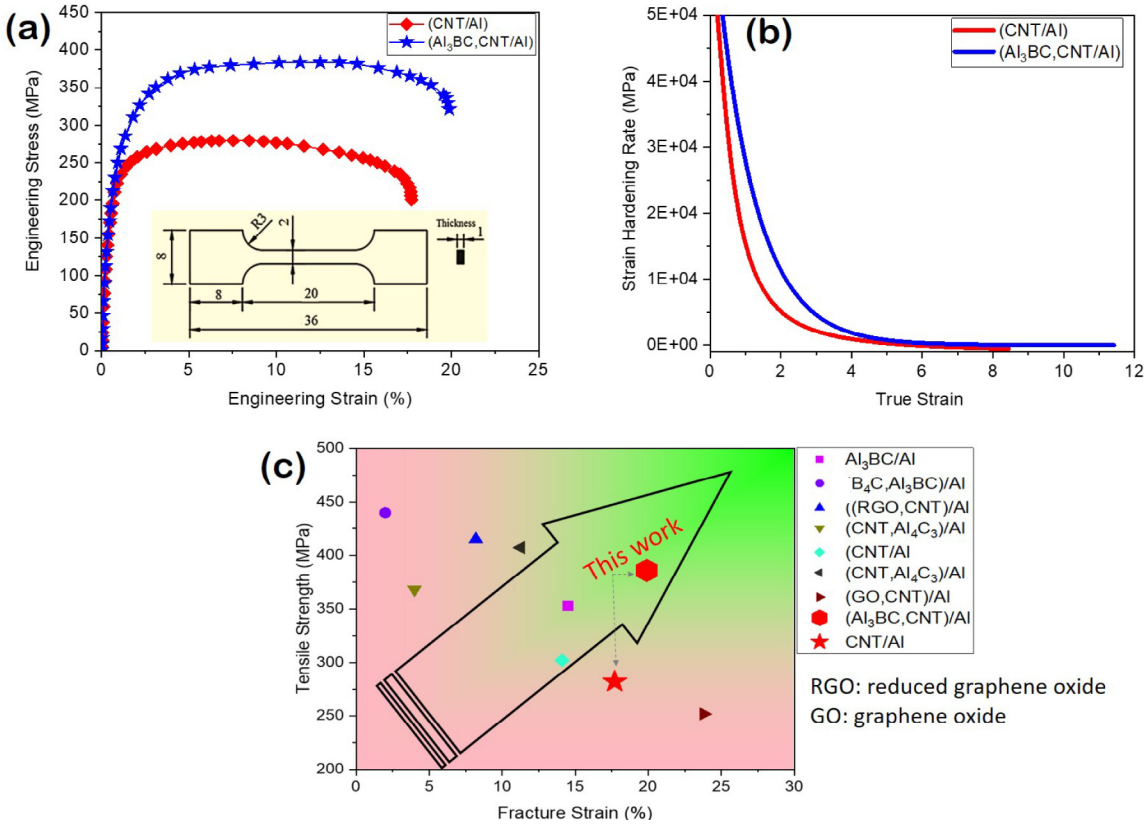

Fig. 6. (a) Engineering tensile stress–strain curves, (b) Strain hardening rate curves of (Al3BC,CNT/Al) and CNT/Al composites. (c) Tensile properties of aluminum composites fabricated by various solid state-based approaches [5,33,35,43–45]. The arrow showing the direction of development the stronger and tougher composites.

and reinforcements, significantly both produce the non-directional short-range local stress for a dislocation to move and dramatically provide long-range interactions with mobile dislocations, exerting a directional long-range back stress opposed to the applied stress in the case of forward loading (Fig. 5).

Shown in Fig. 6a are the tensile stress–strain curves of (Al_3BC, CNT)/Al laminated and CNT/Al composites. Clearly, the (Al_3BC, CNT)/Al laminated composites possess much higher strength than the CNT/Al composites due to vital intragranular and intergranular effects of reinforcements as well as laminated structure. Furthermore, Fig. 6b shows the variation of the strain hardening rate as a function of the true strain, indicating superior maintaining of a high strain-hardening rate for (Al_3BC,CNT)/Al laminated composite. It is attributed to the improved dislocation storage capability of UFG Al because of both having a laminated structure and the in-situ formation of the intragranular Al_3BC nanoparticles. Specifically, the (Al_3BC,CNT)/Al shows a strength of 394 MPa, a uniform elongation of 13.2 % and a total elongation of 19.7 %, about 29 % of the CNT/Al in strength with an increase in total elongation from 17.7 % to 19.5 %, respectively. On the other hand, the uniform elongation of (Al_3BC,CNT)/Al laminated composite is 13.2 %, while that of PM 16 vol% B4C/UFG Al with average grain size of 500 nm is only 3.5 % [40], for PM (0.5wt.%CNT, 2 vol% γ-Al_2O_3) /UFG Al with a unique intragranular dispersion of ultra-short CNTs is about 5.9 % [41]. In consideration of the similarity of the in-situ reinforcements in (Al_3BC,CNT)/UFG Al and 15 vol.%Al_3BC/UFG Al [35], the superior strength and ductility of (Al_3BC,CNT)/UFG Al could only be attributed to the synergetic contribution of intragranular (e.g. caused by in-situ formed Al_3BC, partially formed Al_3C_4) and intergranular strengthening (e.g. arising from CNT, γ-Al_2O_3), estimated to be 1 wt% by the spherical nanoparticles of Al_3BC (Fig. 6c). A synergetic of intragranular and intergranular reinforcements in the elongated Al grains are rendered by the presence of in-situ formed nano-dispersoids, which suggest the promising strengthening effects of Al_3BC benefitting from the strong semi-coherent interface on the matrix. The GBs decorated by CNT and some γ-Al_2O_3 is effectively lost their efficiency in dislocation annihilation by dislocation nucleation in the neighboring matrix grain near the GB, which in turn reduces the magnitude of stress concentration [42], and an increase in critical resolved shear stress as a consequence of harder dislocation motion. It supports the notion that dislocation multiplication and accumulation rather than its annihilation due to recovery was the governing mechanism.

The GBs decorated by CNT and some γ-Al_2O_3 is effectively lost their efficiency in dislocation annihilation, contributing in producing of back stress hardening. While, the reinforcement settled in the Al grains interior increase dislocation blocking, and forest hardening. It is work, namely achieving ultra-high strengthening and toughening efficiency via intragranular/intergranular dispersion engineering, is one step forward from the Jiang et al. [10] work, so that the presence of the array of in-situ formed hybrid nanoparticle-rich zones surrounded by CNT-decorated GBs led to a concurrently enhancement in strength and ductility.

4. Conclusions

Summarily, it is demonstrated that the unique composite, namely the (Al_3BC,CNT)/UFG Al laminated composite exhibits an excellent combined strengthening-ductility effect (strength 394 MPa, elongation 19.7 %), due to the synergetic intragranular/intergranular dispersion, which stand out from most available AMCs. The interface coherency and interfacial bonding between in-situ nano-Al_3BC in the interior of elongated ultrafine Al grains as well as the Al_4C_3 formed partially at the GBs tips could provide a superior strengthening contribution compared with traditional CNT/UFG Al composites. Through a careful combination of in situ and ex situ strengthening techniques, we provided a distribution of support, resulting in the development of dislocation blocks, stress recovery, and forest hardening. This process leads to an increase in the strength and ductility of the composite. The success of our combination and the surprising properties of this unique combination opened new opportunities for research and development of advanced materials with improved equipment and general applications.

Declaration of Competing Interest

The authors declare that they have no known competing financial interests or personal relationships that could have appeared to influence the work reported in this paper.

Appendix A. Supplementary data

Supplementary data to this article can be found online at https://doi.org/10.1016/j.apt.2023.104263.

References

[1] B. Sadeghi, P. Cavaliere, C.I. Pruncu, M. Balog, M. Marques de Castro, R. Chahal, Architectural design of advanced aluminum matrix composites: a review of recent developments, Crit. Rev. Solid State Mater. Sci. (2022) 1–71.
[2] H. Sun, F. Saba, G. Fan, Z. Tan, Z. Li, Micro/nano-reinforcements in bimodal-grained matrix: A heterostructure strategy for toughening particulate reinforced metal matrix composites, Scr. Mater. 217 (2022) 114774.
[3] F. Luo, X. Jiang, H. Sun, D. Mo, Y. Zhang, R. Shu, L. Xue, Microstructures, mechanical and thermal properties of diamonds and graphene hybrid reinforced laminated Cu matrix composites by vacuum hot pressing, Vacuum 207 (2023) 111610.
[4] Z.Y. Xu, C.J. Li, Z. Wang, D. Fang, P. Gao, J.M. Tao, J.H. Yi, J. Eckert, Balancing the strength and ductility of graphene oxide-carbon nanotube hybrid reinforced aluminum matrix composites with bimodal grain distribution, Mater. Sci. Eng. A 796 (2020) 140067.
[5] Z. Li, G. Fan, Q. Guo, Z. Li, Y. Su, D. Zhang, Synergistic strengthening effect of graphene-carbon nanotube hybrid structure in aluminum matrix composites, Carbon 95 (2015) 419–427.
[6] L.-Y. Chen, J.-Q. Xu, H. Choi, M. Pozuelo, X. Ma, S. Bhowmick, J.-M. Yang, S. Mathaudhu, X.-C. Li, Processing and properties of magnesium containing a dense uniform dispersion of nanoparticles, Nature 528 (7583) (2015) 539–543.
[7] G. Fan, Q. Liu, A. Kondo, M. Naito, K. Kushimoto, J. Kano, Z. Tan, Z. Li, Self-assembly of nanoparticles and flake powders by flake design strategy via dry particle coating, Powder Technol. 418 (2023) 118294.
[8] B. Sadeghi, G. Fan, Z. Tan, Z. Li, A. Kondo, M. Naito, Smart Mechanical Powder Processing for Producing Carbon Nanotube Reinforced Aluminum Matrix Composites, Kona Powder Part. J. (2022) 2022004.
[9] L. Ma, X. Zhang, B. Pu, D. Zhao, C. He, N. Zhao, Achieving the strength-ductility balance of boron nitride nanosheets/Al composite by designing the synergistic transition interface and intragranular reinforcement distribution, Compos. B Eng. 246 (2022) 110243.
[10] L. Jiang, H. Yang, J.K. Yee, X. Mo, T. Topping, E.J. Lavernia, J.M. Schoenung, Toughening of aluminum matrix nanocomposites via spatial arrays of boron carbide spherical nanoparticles, Acta Mater. 103 (2016) 128–140.
[11] J. Wan, J. Yang, X. Zhou, B. Chen, J. Shen, K. Kondoh, J. Li, Superior tensile properties of graphene/Al composites assisted by in-situ alumina nanoparticles, Carbon 204 (2023) 447–455.
[12] Y. Zhang, X. Li, Bioinspired, graphene/Al2O3 doubly reinforced aluminum composites with high strength and toughness, Nano Lett. 17 (11) (2017) 6907–6915.
[13] B. Sadeghi, P.D. Cavaliere, Reviewing the integrated design approach for augmenting strength and toughness at macro- and micro-scale in high-performance advanced composites, Materials 16 (17) (2023) 5745.
[14] B. Sadeghi, P. Cavaliere, Progress of Flake Powder Metallurgy Research, Metals 11 (6) (2021) 931.
[15] G.L. Fan, R. Xu, Z.Q. Tan, D. Zhang, Z.Q. Li, Development of flake powder metallurgy in fabricating metal matrix composites: A Review, Acta Metallurgica Sinica-English Letters 27 (5) (2014) 806–815.
[16] L. Jiang, Z.Q. Li, G.L. Fan, D. Zhang, A flake powder metallurgy approach to Al2O3/Al biomimetic nanolaminated composites with enhanced ductility, Scr. Mater. 65 (5) (2011) 412–415.
[17] B. Sadeghi, P. Cavaliere, M. Balog, C.I. Pruncu, A. Shabani, Microstructure dependent dislocation density evolution in micro-macro rolled Al2O3/Al laminated composite, Mater. Sci. Eng. A 830 (2022) 142317.
[18] B. Sadeghi, P. Cavaliere, C.I. Pruncu, Architecture dependent strengthening mechanisms in graphene/Al heterogeneous lamellar composites, Mater Charact 111913 (2022).

[19] C. He, N. Zhao, C. Shi, S. Song, Mechanical properties and microstructures of carbon nanotube-reinforced Al matrix composite fabricated by in situ chemical vapor deposition, J. Alloy. Compd. 487 (1–2) (2009) 258–262.
[20] L.P. Yan, Z.Q. Tan, G. Ji, Z.Q. Li, G.L. Fan, D. Schryvers, A.D. Shan, D. Zhang, A quantitative method to characterize the Al4C3-formed interfacial reaction: The case study of MWCNT/Al composites, Mater Charact 112 (2016) 213–218.
[21] G. Williamson, R. Smallman III, Dislocation densities in some annealed and cold-worked metals from measurements on the X-ray debye-scherrer spectrum, Phil. Mag. 1 (1) (1956) 34–46.
[22] D. Lahiri, S.R. Bakshi, A.K. Keshri, Y. Liu, A. Agarwal, Dual strengthening mechanisms induced by carbon nanotubes in roll bonded aluminum composites, Mater. Sci. Eng. A 523 (1–2) (2009) 263–270.
[23] Y. Lin, B. Yao, Z. Zhang, Y. Li, Y. Sohn, J.M. Schoenung, E.J. Lavernia, Strain Energy During Mechanical Milling: Part I, Mathematical Modeling, Metallurgical and Materials Transactions A 43 (11) (2012) 4247–4257.
[24] P.P. Chattopadhyay, I. Manna, S. Talapatra, S.K. Pabi, A mathematical analysis of milling mechanics in a planetary ball mill, Mater. Chem. Phys. 68 (1) (2001) 85–94.
[25] S. Kleiner, F. Bertocco, F. Khalid, O. Beffort, Decomposition of process control agent during mechanical milling and its influence on displacement reactions in the Al–TiO2 system, Mater. Chem. Phys. 89 (2–3) (2005) 362–366.
[26] R. Dabouz, M. Bendoumia, L. Belaid, M. Azzaz, Dissolution of Al 6%wt c mixture using mechanical alloying, Defect and Diffusion Forum 391 (2019) 82–87.
[27] M. Kubota, P. Cizek, Synthesis of Al3BC from mechanically milled and spark plasma sintered Al–MgB2 composite materials, J. Alloy. Compd. 457 (1) (2008) 209–215.
[28] Y. Zhao, X. Ma, X. Zhao, H. Chen, X. Liu, Enhanced aging kinetic of Al3BC/6061 Al composites and its micro-mechanism, J. Alloy. Compd. 726 (2017) 1053–1061.
[29] Y. Zhao, Z. Qian, X. Liu, Identification of novel dual-scale Al3BC particles in Al based composites, Mater. Des. 93 (2016) 283–290.
[30] Y. Jiang, Z. Tan, G. Fan, Z. Zhang, D.-B. Xiong, Q. Guo, Z. Li, D. Zhang, Nucleation and growth mechanisms of interfacial carbide in graphene nanosheet/Al composites, Carbon 161 (2020) 17–24.
[31] B. Sadeghi, P. Cavaliere, CNTs reinforced Al-based composites produced via modified flake powder metallurgy, J. Mater. Sci. 57 (4) (2022) 2550–2566.
[32] H. Wei, Z.Q. Li, D.B. Xiong, Z.Q. Tan, G.L. Fan, Z. Qin, D. Zhang, Towards strong and stiff carbon nanotube-reinforced high-strength aluminum alloy composites through a microlaminated architecture design, Scr. Mater. 75 (2014) 30–33.
[33] Q. Hu, W. Guo, P. Xiao, J. Yao, First-principles investigation of mechanical, electronic, dynamical, and thermodynamic properties of Al3BC, Phys. B Condens. Matter 616 (2021) 413127.
[34] T. Tsuchida, T. Kan, Synthesis of Al3BC in air from mechanically activated Al/B/C powder mixtures, J. Eur. Ceram. Soc. 19 (9) (1999) 1795–1799.
[35] Y. Zhao, Z. Qian, X. Ma, H. Chen, T. Gao, Y. Wu, X. Liu, Unveiling the Semicoherent Interface with Definite Orientation Relationships between Reinforcements and Matrix in Novel Al3BC/Al Composites, ACS Appl. Mater. Interfaces 8 (41) (2016) 28194–28201.
[36] Y. Zhao, X. Ma, H. Chen, X. Zhao, X. Liu, Preferred orientation and interfacial structure in extruded nano-Al3BC/6061 Al, Mater. Des. 131 (2017) 23–31.
[37] B. Chen, L. Jia, S. Li, H. Imai, M. Takahashi, K. Kondoh, In Situ Synthesized Al4C3Nanorods with Excellent Strengthening Effect in Aluminum Matrix Composites, Adv. Eng. Mater. 16 (8) (2014) 972–975.
[38] W. Zhou, T. Yamaguchi, K. Kikuchi, N. Nomura, A. Kawasaki, Effectively enhanced load transfer by interfacial reactions in multi-walled carbon nanotube reinforced Al matrix composites, Acta Mater. 125 (2017) 369–376.
[39] M. Balog, P. Krizik, M. Nosko, Z. Hajovska, M. Victoria Castro Riglos, W. Rajner, D.-S. Liu, F. Simancik, Forged HITEMAL: Al-based MMCs strengthened with nanometric thick Al 2 O 3 skeleton, Mater. Sci. Eng. A 613 (2014) 82–90.
[40] X. Kai, Z. Li, G. Fan, Q. Guo, Z. Tan, W. Zhang, Y. Su, W. Lu, W.-J. Moon, D. Zhang, Strong and ductile particulate reinforced ultrafine-grained metallic composites fabricated by flake powder metallurgy, Scr. Mater. 68 (8) (2013) 555–558.
[41] Q. Liu, G. Fan, Z. Tan, Q. Guo, D. Xiong, Y. Su, Z. Li, D. Zhang, Reinforcement with intragranular dispersion of carbon nanotubes in aluminum matrix composites, Compos. B Eng. 217 (2021) 108915.
[42] Z. Li, L. Zhao, Q. Guo, Z. Li, G. Fan, C. Guo, D. Zhang, Enhanced dislocation obstruction in nanolaminated graphene/Cu composite as revealed by stress relaxation experiments, Scr. Mater. 131 (2017) 67–71.
[43] L. Jiang, Z.Q. Li, G.L. Fan, L.L. Cao, D. Zhang, Strong and ductile carbon nanotube/aluminum bulk nanolaminated composites with two-dimensional alignment of carbon nanotubes, Scr. Mater. 66 (6) (2012) 331–334.
[44] B. Sadeghi, J. Qi, X. Min, P. Cavaliere, Modelling of strain rate dependent dislocation behavior of CNT/Al composites based on grain interior/grain boundary affected zone (GI/GBAZ), Mater. Sci. Eng. A 820 (2021) 141547.
[45] Z. Zhang, G. Fan, Z. Tan, H. Zhao, Y. Xu, D. Xiong, Z. Li, Bioinspired multiscale Al2O3-rGO/Al laminated composites with superior mechanical properties, Compos. B Eng. 217 (2021) 108916.